HHS Public Access

Author manuscript

*Nature*. Author manuscript; available in PMC 2011 December 02.

Published in final edited form as:

*Nature*. 2011 June 2; 474(7349): 100–104. doi:10.1038/nature09986.

# Glutamate induces *de novo* growth of functional spines in developing cortex

**Hyung-Bae Kwon** and **Bernardo L. Sabatini***

Howard Hughes Medical Institute, Department of Neurobiology, Harvard Medical School, Boston, Massachusetts 02115

## Abstract

Mature cortical pyramidal neurons receive excitatory inputs onto small protrusions emanating from their dendrites called spines. Spines undergo activity-dependent remodeling, stabilization, and pruning during development and similar structural changes can be triggered by learning and changes in sensory experiences[1–4]. However, the biochemical triggers and mechanisms of *de novo* spine formation in the developing brain and the functional significance of new spines to neuronal connectivity are largely unknown. We developed an approach to induce and monitor *de novo* spine formation in real-time using combined two-photon laser-scanning microscopy and two-photon laser uncaging of glutamate. Our data demonstrate that, in mouse cortical layer 2/3 pyramidal neurons, glutamate is sufficient to trigger *de novo* spine growth from the dendrite shaft in a location-specific manner. We find that glutamate-induced spinogenesis requires opening of NMDA-type glutamate receptors and activation of PKA but is independent of CaMKII and TrkB receptors. Furthermore, newly formed spines express glutamate receptors and are rapidly functional such that they transduce presynaptic activity into postsynaptic signals. Together, our data demonstrate that early neural connectivity is shaped by activity in a spatially precise manner and that nascent dendrite spines are rapidly functionally incorporated into cortical circuits.

During post-natal development, the formation and elimination of glutamatergic synapses are thought to be reflected in the growth and retraction of dendritic spines. In cortical pyramidal neurons, waves of new spine growth (spinogenesis) and synapse formation (synaptogenesis) occur at specific developmental stages, followed by pruning as the brain matures[5]. Many signals have been proposed to trigger and regulate *de novo* spine growth in a developing circuit including neurotrophins, neurotransmitters, and cell adhesion molecules[6–9]. To uncover the triggers for and mechanisms of spinogenesis, we imaged dendrites of EGFP-expressing cortical layer 2/3 pyramidal neurons while releasing glutamate at a specific dendritic location by 2-photon laser induced-photolysis of MNI (4-methoxy-7-



*Corresponding author: Bernardo L. Sabatini, Howard Hughes Medical Institute, Department of Neurobiology, Harvard Medical School, 220 Longwood Ave., Boston, MA 02115, bsabatini@hms.harvard.edu.

**Author contributions**

HBK and BS designed the experiments and wrote the paper. HBK performed all the experiments, analyzed the data (other than spine counting by a blind, third party observer), and prepared the figures.

nitroindolinyl)-glutamate (Fig. 1). Analysis was performed in acute cortical brain slices from young mice (postnatal day (P) 8~12), a time period in which spinogenesis occurs *in vivo*[10].

Stimulation near edge of a dendrite with forty 0.5 ms laser pulses at 0.5 Hz in a $Mg^{2+}$-free extracellular solution induced growth of a new spine in ~14% of cases (Fig. 1a-d, Supplemental Fig. 1), showing the possibility of *de novo* spinogenesis induced by glutamate exposure[11]. Increasing stimulation frequency and laser pulse duration while maintaining the total number of stimuli at 40 increased the rate of spinogenesis such that at 5 Hz with 4 ms duration, a maximal success rate of ~50% was achieved (Fig. 1c). Nascent spines arose from the dendrite where glutamate was released with high specificity (Fig. 1b) such that more than 70% of them grew within 1 μm of the uncaging spot (Fig. 1e) and 94% of them grew on the side of the dendrite exposed to glutamate.

In 128 of 132 examples of glutamate-induced spinogenesis, the spine was seen to emerge without a filopodial stage (See Supplementary Fig. 2a for an exception). Instead, spine growth occurred incrementally but explosively such that the spine head volume increased from 10 to 90% of maximum within 11.8 ± 1.5 pulses of glutamate (5.9 ± 0.8 sec at 2 Hz stimulation) (Fig. 2a-c, Supplementary Fig. 3). The final sizes and lengths of the newborn spines were heterogeneous but not different from those of pre-existing neighboring spines (Fig. 2d-e). The lifetime of newly formed spines was variable such that ~20% lasted less than 2 minutes but those that lasted 5 minutes were stable and remained for at least 30 minutes (Supplementary Fig. 4). Thus, these newly formed spines either did not require continued exposure to glutamate for maintenance or they received glutamate from an alternative source such as an axonal bouton.

Glutamate-induced spinogenesis was restricted within postnatal developmental such that its efficiency diminished by P14–15 and it failed to occur by P19–20 (Supplementary Fig. 5). This was not due to decreased glutamate receptor activation in older animals since the uncaging-evoked EPSC was larger at P19~20 than at P10~12 (Supplementary Fig. 6).

Previous ultrastructural studies have revealed a high frequency of dendrite shaft synapses in hippocampus in early postnatal life that decreases as spinogenesis occurs[12], leading to a model of synaptic development in which synapses are initially formed directly onto the dendritic shaft and a spine subsequently grows from this point with the synapse attached. On the other hand, rapid movement of a physically connected spine head and axonal bouton together through a complex neuropil is difficult to reconcile with the high density of crossing axons and dendrites[13]. Our data demonstrate that glutamate uncaging-induced spinogenesis occurs with high spatial specificity and probability on the side of the dendrite exposed to glutamate. These findings place a lower limit of ~ 1/μm for the density of dendritic shaft synapses required to support this model of spinogenesis. To estimate the number of dendritic shaft synapses, $Ca^{2+}$ imaging was performed in conditions in which the majority of synapses formed onto a stretch of dendrite were activated (~90%, Supplementary Fig. 7). Under these conditions, we observed hotspots of $Ca^{2+}$ influx in spineless stretches of dendrite at a density of 0.05/μm. This corresponds to a density of dendritic shaft synapses containing NMDARs that is approximately 20 fold less than

necessary to explain the specificity and efficiency of glutamate-induced spinogenesis (see Supplementary Fig. 7 for further discussion).

The high success rate of spinogenesis induced by glutamate uncaging allows identification of the signaling pathways that couple activity to spine growth (Fig. 3). Previous analyses of spine generation induced by electrical stimulation indicate a requirement for NMDA-type glutamate receptors (NMDARs) in this process[14],[15] and at this age NMDARs are found throughout the dendrite (Supplementary Fig. 8). Preventing NMDAR activation with the antagonist CPP nearly abolished spinogenesis whereas it was unaffected by inhibiting AMPA/kainate glutamate receptors with NBQX (Fig. 3a). The voltage-gated sodium channel antagonist TTX also did not affect spinogenesis, discarding the possibility that postsynaptic action potentials are necessary. Addition of extracellular $Mg^{2+}$ significantly decreased the success rate, suggesting that the degree of current flux through NMDARs plays a crucial role in triggering spine formation. Blocking either mGluR1 or mGluR5 using CPCCOEt or MPEP or with the less selective group I mGluR antagonist AIDA demonstrated that neither was strictly necessary for spinogenesis. Lastly, depleting $Ca^{2+}$ stores with cyclopiazonic acid (CPA) or thapsigargin (TG) significantly inhibited spine formation. Thus, our data indicate that NMDARs with additional contributions from intracellular stores provide the coupling between glutamate and activation of intracellular pathways responsible for spinogenesis.

We further considered intracellular signaling pathways that might be activated in a spatially-delimited fashion by glutamate and could provide the spatial information necessary for local spine growth. Previous studies of long-term potentiation (LTP) and associated spine enlargement in older animals demonstrated a need for activation of CaMKII or signaling via neurotrophin receptor tyrosine kinases such as the BDNF receptor TrkB[16]–[19]. However, we find that activity-dependent spinogenesis is unaffected by the kinase inhibitors KN-62, KN-93, and K252a, indicating independence from CaMKII and TrkB signaling (Fig. 3a).

The cAMP-activated kinase PKA is required for LTP induction in younger neurons[20] and gradients in its concentration can be maintained over micron length scales[21]. Raising cAMP concentration by applying the adenylate cyclase activator forskolin was not sufficient to generate spines on its own (n=3, data not shown), but glutamate uncaging in its presence increased the spinogenesis success rate to ~80% (Fig. 3a). In the presence of forskolin, multiple spines often grow per induction attempt (Fig. 3b and c), including at sites more distant from the uncaging location (Fig. 3d). In addition, the PKA inhibitor H-89 prevented new spine growth (Fig. 3a), indicating that PKA activity is necessary but not sufficient for spinogenesis.

The small guanosine triphosphatase Ras is activated by $Ca^{2+}$ influx through NMDARs and signals via mitogen-activated protein kinase (MAPK) to promote LTP induction[17],[22]. We found that the MAPK pathway was necessary for spinogenesis since the success rate was significantly reduced by blocking the upstream activator of MEK1/2 with U0126 and MEK1 with PD98059 (Fig. 3a). In pyramidal neurons, activated Ras diffuses from active spines to neighboring spines and heterosynaptically facilitates plasticity[17]. To examine if a similar phenomenon potentiates spinogenesis, we delivered a “priming” stimulus to a pre-existing

spine (40 pulses at 2 Hz, Fig. 3e) and then a "test" stimulus to the dendritic shaft within 1~2 minutes. In contrast to previous studies of older neurons in hippocampus[16–18], we found no consistent increases in volume of the existing spine in response to this priming stimulus (Fig. 3f), supporting that spinogenesis is not simply due to the growth of an undetectable preexisting spine. Nevertheless, the success rate of spine generation was enhanced by the priming stimulus in a MEK1/2 dependent manner such that the low level of spinogenesis evoked by a 0.5 Hz test stimulus was increased. In contrast, the priming stimulus did not increase the success rate when the test stimulus was delivered at 2Hz (Fig. 3g), indicating that the priming protocol shifted the induction threshold for spinogenesis.

With the exception of the NMDAR and PKA antagonists, none of the pharmacological manipulations that altered spinogenesis rates affected dendritic currents or $Ca^{2+}$ transients (Supplementary Fig. 8). As expected, CPP largely abolished the $Ca^{2+}$ transient and the prolonged phase of the currents. Consistent with a facilitation of $Ca^{2+}$ influx through NMDARs by PKA[23,24], H-89 lowered dendritic $Ca^{2+}$ transients by ~20% (Supplementary Table 1). However, this effect is insufficient to explain the near abolishment of spinogenesis since the rate of spinogenesis evoked by 0.5 ms uncaging pulses in control conditions was higher than that evoked by 4 ms pulses in H-89, despite eliciting smaller dendritic $Ca^{2+}$ transients (Supplementary Fig. 8 and Table 1).

We examined whether synaptic activity generated new spines in cortical tissue from young mice via similar pathways. In normal extracellular $Mg^{2+}$, high-frequency (100 pulses at 100 Hz, delivered twice separated by 10 seconds) but not low-frequency (10 Hz) electrical tetani rapidly triggered new spine growth (Fig. 3h-i). Blockade of NMDARs or PKA prevented this synaptically-evoked spine growth (Fig. 3i) as well as spontaneous new spine growth that occurred when NMDAR activation was increased by removing extracellular $Mg^{2+}$ and blocking inhibitory $GABA_A$ receptors (Supplementary Fig. 9). Hence, multiple experimental paradigms demonstrate that activity-dependent spinogenesis in developing cortex requires NMDAR- and PKA-dependent signaling.

In order to determine if nascent spines detect synaptically-released glutamate and are functionally incorporated into the circuit, we generated new spines by high frequency stimulation (HFS) and examined their synaptic responses using optical quantal analysis of synaptic properties. A whole-cell recording was obtained and the probability and amplitude of synaptically-evoked NMDAR-mediated $Ca^{2+}$ transients in the spine head were monitored (Fig. 4a). Using the $Ca^{2+}$ sensitive green fluorophore Fluo-5F, we detected stimulus-evoked $Ca^{2+}$ transients in the heads of newly-grown spines (Fig. 4b-c), demonstrating that they sense synaptic activity within a neural circuit within 30 min after growth. Similar results were obtained in 5 of 7 new spines and in 11 of 16 preexisting spines. Analysis of the spines in which an evoked $Ca^{2+}$ transient could be detected indicated that nascent spines displayed smaller and less frequent synaptically-evoked $Ca^{2+}$ transients than pre-existing spines (Fig. 4d-e). Similar results were obtained for new spines that grew in response to glutamate uncaging and probed using a glass stimulating electrode placed near the spine (Supplementary Fig. 10).

The AMPAR and NMDAR content of new spines was characterized using glutamate uncaging following HFS-induced spinogenesis. In all cases, we detected fast uncaging-evoked postsynaptic currents (uEPSCs) at a holding potential of -60 mV and large prolonged uEPSCs at +40 mV (Fig. 4g), consistent with AMPAR- and NMDAR-mediated currents previously characterized in these cells[25]. Similarly, uncaging-evoked $Ca^{2+}$ transients were clearly visible at -60 mV (Fig. 4h) but were larger at +40 mV (not shown), consistent with the known properties of NMDAR-mediated $Ca^{2+}$ influx. Despite similar-sized AMPAR-uEPSCs in new and preexisting spines, NMDAR-uEPSCs and $Ca^{2+}$ influx were significantly lower in nascent spines compared to pre-existing spines (Fig. 4g-h). Therefore, the smaller $Ca^{2+}$ transients measured in nascent spines by synaptic activation likely reflects a lower number of postsynaptic NMDARs.

In this study, we established a protocol for the reliable and spatiotemporally precise induction of spinogenesis. These experiments demonstrate that glutamate is sufficient to trigger rapid spine formation and suggest that neurons use glutamate release to establish circuit wiring. Thus, these data support the hypothesis that axonal growth and glutamate release may be the triggering event in synapse formation such that axonal bouton localization is an important early step for precise neuronal circuit formation[10,26]. Given the involvement of NMDARs, $Ca^{2+}$ stores, cAMP, PKA, and MAPK in activity-dependent spinogenesis, it is likely that many neuromodulators that regulate these molecules may influence the capacity or threshold for new spine formation. For instance, activation of dopaminergic, serotonergic, or adrenergic receptors that signal via $G\alpha_s$ may facilitate spinogenesis, whereas receptors that activate $G\alpha_i$-coupled signaling may function as inhibitory signals.

Lastly, we provide experimental evidence that spines that grow *de novo* in developing cortical tissue become rapidly functionally integrated into the circuit such that they sense synaptically-released glutamate via AMPARs and NMDARs. Whether these nascent spines are rapidly physically associated with a presynaptic bouton and display the ultrastructural correlates of a synapse are unknown[27–30]. Our results indicate that spines can grow *de novo* without the need for a filopodial and likely without a dendritic-shaft synapse stage. In total, this study demonstrates that synaptic activity can rapidly modify neuronal connectivity with high accuracy by generating new circuit elements.

## Methods Summary

All procedures on animals followed protocols approved by the Harvard Standing Committee on Animal Care and National Institutes of Health guidelines. *In utero* electroporation of EGFP was performed at E15.5 in C57BL/6 mice. All studies were performed on Layer 2/3 pyramidal neurons in acute coronal slices identified based on their characteristic morphology and position in the slice as well as by the expression of GFP. 2-photon glutamate uncaging and imaging was performed using custom microscopes. To induce spine growth, 40 uncaging pulses were delivered at varying frequencies to a spot ~0.5 μm from the edge of the dendrite. Synaptically-induced spine growth was triggered with two high-frequency stimuli (100×100Hz) separated by 10 sec delivered via a bipolar electrode positioned ~30 μm from the target dendrite. For $Ca^{2+}$ imaging, neurons were loaded through

the whole-cell recording electrode with Alexa Fluor-594 (20 μM) and Fluo-5F (300 μM) and the amplitude of fluorescence transients were quantified as a fraction of the maximal green fluorescence achieved in saturating $Ca^{2+}$ concentrations. For optical quantal analysis, the synapse associated with a visualized spine was stimulated using a closely positioned glass electrode. The position of the electrode and stimulus intensity were adjusted until (1) $Ca^{2+}$ transients were evoked in the spine head that demonstrated stochastic failures and successes and (2) $Ca^{2+}$ transients in other spines and the dendritic shaft in the field of view were not evoked. The Fisher's exact test was used to compare the efficacy of spinogenesis across conditions. For each spinogenesis trial, an observer blind to the experimental condition was asked to identify if (1) a new spine had grown and (2), if so, how many spines had grown.

## Supplementary Material

Refer to Web version on PubMed Central for supplementary material.

## Acknowledgments

We thank members of the Sabatini lab for their constructive comments on the manuscript and assistance with data analysis routines. We are grateful to S. Nazia for technical support and for acting as the blind evaluator. This work was supported by a SFARI grant from the Simons Foundation (to B.L.S.)

## References

1. Grutzendler J, Kasthuri N, Gan WB. Long-term dendritic spine stability in the adult cortex. Nature. 2002; 420:812–816. [PubMed: 12490949]
2. Hofer SB, Mrsic-Flogel TD, Bonhoeffer T, Hubener M. Experience leaves a lasting structural trace in cortical circuits. Nature. 2009; 457:313–317. [PubMed: 19005470]
3. Trachtenberg JT, et al. Long-term in vivo imaging of experience-dependent synaptic plasticity in adult cortex. Nature. 2002; 420:788–794. [PubMed: 12490942]
4. Zuo Y, Yang G, Kwon E, Gan WB. Long-term sensory deprivation prevents dendritic spine loss in primary somatosensory cortex. Nature. 2005; 436:261–265. [PubMed: 16015331]
5. Rakic P, Bourgeois JP, Eckenhoff MF, Zecevic N, Goldman-Rakic PS. Concurrent overproduction of synapses in diverse regions of the primate cerebral cortex. Science. 1986; 232:232–235. [PubMed: 3952506]
6. Dalva MB, McClelland AC, Kayser MS. Cell adhesion molecules: signalling functions at the synapse. Nat Rev Neurosci. 2007; 8:206–220. [PubMed: 17299456]
7. Scheiffele P. Cell-cell signaling during synapse formation in the CNS. Annu Rev Neurosci. 2003; 26:485–508. [PubMed: 12626697]
8. Sudhof TC. Neuroligins and neurexins link synaptic function to cognitive disease. Nature. 2008; 455:903–911. [PubMed: 18923512]
9. Yuste R, Bonhoeffer T. Genesis of dendritic spines: insights from ultrastructural and imaging studies. Nat Rev Neurosci. 2004; 5:24–34. [PubMed: 14708001]
10. Miller M, Peters A. Maturation of rat visual cortex. II. A combined Golgi-electron microscope study of pyramidal neurons. J Comp Neurol. 1981; 203:555–573. [PubMed: 7035504]
11. Richards DA, et al. Glutamate induces the rapid formation of spine head protrusions in hippocampal slice cultures. Proc Natl Acad Sci U S A. 2005; 102:6166–6171. [PubMed: 15831587]
12. Fiala JC, Feinberg M, Popov V, Harris KM. Synaptogenesis via dendritic filopodia in developing hippocampal area CA1. J Neurosci. 1998; 18:8900–8911. [PubMed: 9786995]
13. Sorra KE, Fiala JC, Harris KM. Critical assessment of the involvement of perforations, spinules, and spine branching in hippocampal synapse formation. J Comp Neurol. 1998; 398:225–240. [PubMed: 9700568]

14. Engert F, Bonhoeffer T. Dendritic spine changes associated with hippocampal long-term synaptic plasticity. Nature. 1999; 399:66–70. [PubMed: 10331391]
15. Maletic-Savatic M, Malinow R, Svoboda K. Rapid dendritic morphogenesis in CA1 hippocampal dendrites induced by synaptic activity. Science. 1999; 283:1923–1927. [PubMed: 10082466]
16. Harvey CD, Svoboda K. Locally dynamic synaptic learning rules in pyramidal neuron dendrites. Nature. 2007; 450:1195–1200. [PubMed: 18097401]
17. Harvey CD, Yasuda R, Zhong H, Svoboda K. The spread of Ras activity triggered by activation of a single dendritic spine. Science. 2008; 321:136–140. [PubMed: 18556515]
18. Matsuzaki M, Honkura N, Ellis-Davies GC, Kasai H. Structural basis of long-term potentiation in single dendritic spines. Nature. 2004; 429:761–766. [PubMed: 15190253]
19. Tanaka J, et al. Protein synthesis and neurotrophin-dependent structural plasticity of single dendritic spines. Science. 2008; 319:1683–1687. [PubMed: 18309046]
20. Yasuda H, Barth AL, Stellwagen D, Malenka RC. A developmental switch in the signaling cascades for LTP induction. Nat Neurosci. 2003; 6:15–16. [PubMed: 12469130]
21. Zaccolo M, Pozzan T. Discrete microdomains with high concentration of cAMP in stimulated rat neonatal cardiac myocytes. Science. 2002; 295:1711–1715. [PubMed: 11872839]
22. Di Cristo G, et al. Requirement of ERK activation for visual cortical plasticity. Science. 2001; 292:2337–2340. [PubMed: 11423664]
23. Chalifoux JR, Carter AG. GABAB receptors modulate NMDA receptor calcium signals in dendritic spines. Neuron. 66:101–113. [PubMed: 20399732]
24. Skeberdis VA, et al. Protein kinase A regulates calcium permeability of NMDA receptors. Nat Neurosci. 2006; 9:501–510. [PubMed: 16531999]
25. Busetto G, Higley MJ, Sabatini BL. Developmental presence and disappearance of postsynaptically silent synapses on dendritic spines of rat layer 2/3 pyramidal neurons. J Physiol. 2008; 586:1519–1527. [PubMed: 18202095]
26. Hamori J. The inductive role of presynaptic axons in the development of postsynaptic spines. Brain Res. 1973; 62:337–344. [PubMed: 4760510]
27. Zito K, Scheuss V, Knott G, Hill T, Svoboda K. Rapid functional maturation of nascent dendritic spines. Neuron. 2009; 61:247–258. [PubMed: 19186167]
28. De Roo M, Klauser P, Mendez P, Poglia L, Muller D. Activity-dependent PSD formation and stabilization of newly formed spines in hippocampal slice cultures. Cereb Cortex. 2008; 18:151–161. [PubMed: 17517683]
29. Nagerl UV, Kostinger G, Anderson JC, Martin KA, Bonhoeffer T. Protracted synaptogenesis after activity-dependent spinogenesis in hippocampal neurons. J Neurosci. 2007; 27:8149–8156. [PubMed: 17652605]
30. Knott GW, Holtmaat A, Wilbrecht L, Welker E, Svoboda K. Spine growth precedes synapse formation in the adult neocortex in vivo. Nat Neurosci. 2006; 9:1117–1124. [PubMed: 16892056]

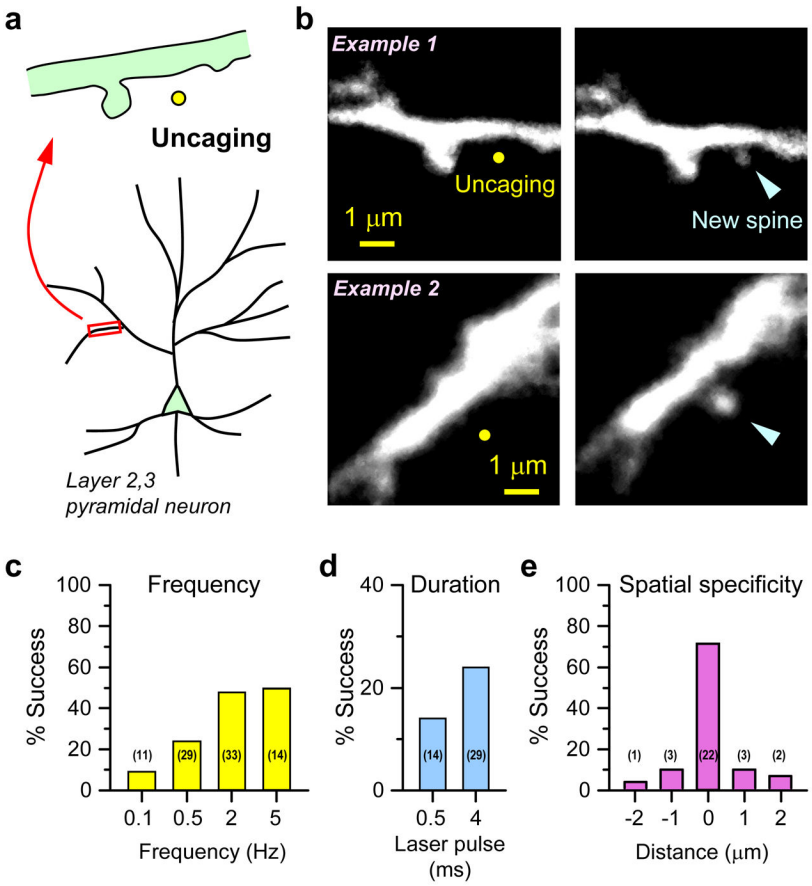


**Figure 1.** ***De novo*** **spine generation is induced by glutamate uncaging**

**(a)** Dendrites of EGFP-expressing neurons in acute slices from P8~12 mice were visualized with 2PLSM and glutamate was released by photolysis of caged glutamate near a low-spine density section of dendrite.

**(b)** Examples of *de novo* spine formation induced by photolytic release of glutamate (40 pulses of MNI-glutamate uncaging at 2 Hz in $Mg^{2+}$-free ACSF). Yellow circles mark the uncaging spots and arrowheads mark new spines.

**(c-e)** Most new spines grew near the uncaging spot and the success percentage depended on the frequency (**c**, laser pulse duration=4 ms) and duration (**d**, stimulation frequency=0.5 Hz) of glutamate uncaging. Experiment numbers for each bar are indicated in parentheses.

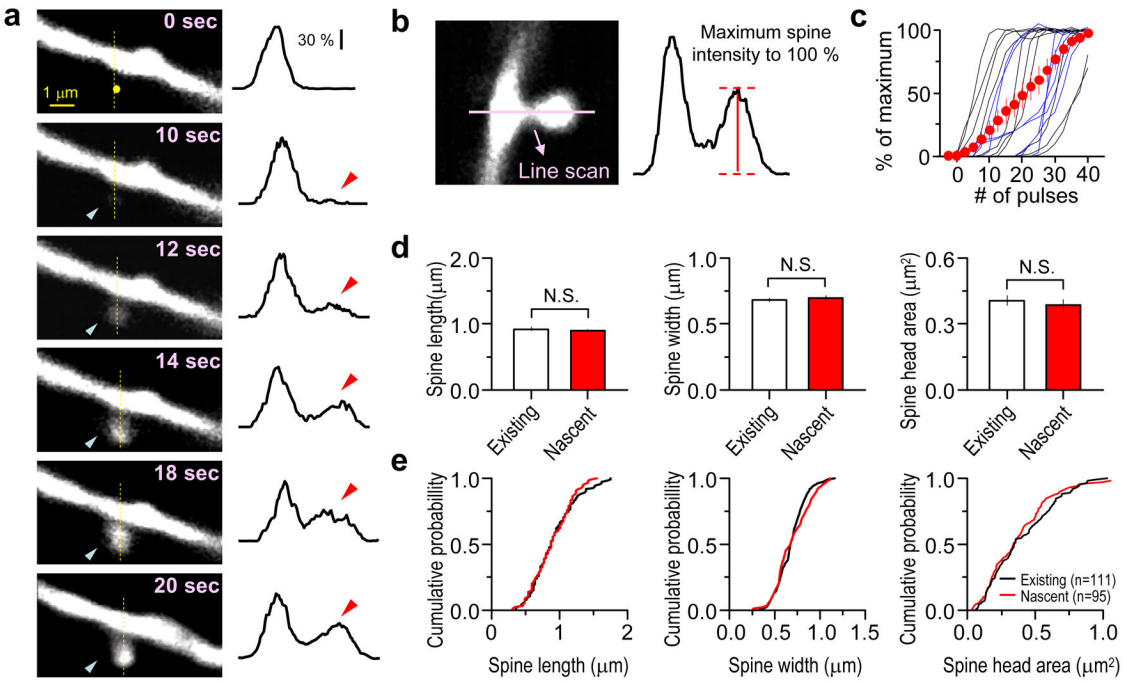


**Figure 2. New spines grow rapidly and acquire morphology similar to pre-existing spines**

**(a)** *left*, Time-lapse images of spine formation during glutamate uncaging (40 pulses, 2 Hz) showing the uncaging spot (yellow circle) and nascent spine (blue arrowhead). *right*, Fluorescence intensity profiles along the yellow line reveal that the spine head fluorescence increases gradually but rapidly (red arrowhead).

**(b)** Illustration of the measurement of spine head fluorescence during spinogenesis as a percentage of the maximum fluorescence intensity reached.

**(c)** Time course of individual (black, 2Hz; blue, 0.5 Hz) and average (red) fluorescence intensity increases during spinogenesis (n=17). Error bars: SEM.

**(d)** Average of apparent spine length, width, and head area from nascent (n=95) and neighboring existing (n=111) spines (existing and nascent: length: 0.92 ± 0.03 μm, 0.89 ± 0.03 μm, $p>0.1$; width: 0.68 ± 0.02 μm, 0.70 ± 0.02 μm, $p>0.1$; head area: 0.41 ± 0.02 $\mu m^2$, 0.38 ± 0.03 $\mu m^2$, $p>0.1$).

**(e)** Cumulative distributions demonstrating that the morphology of pre-existing and nascent spines are not different.

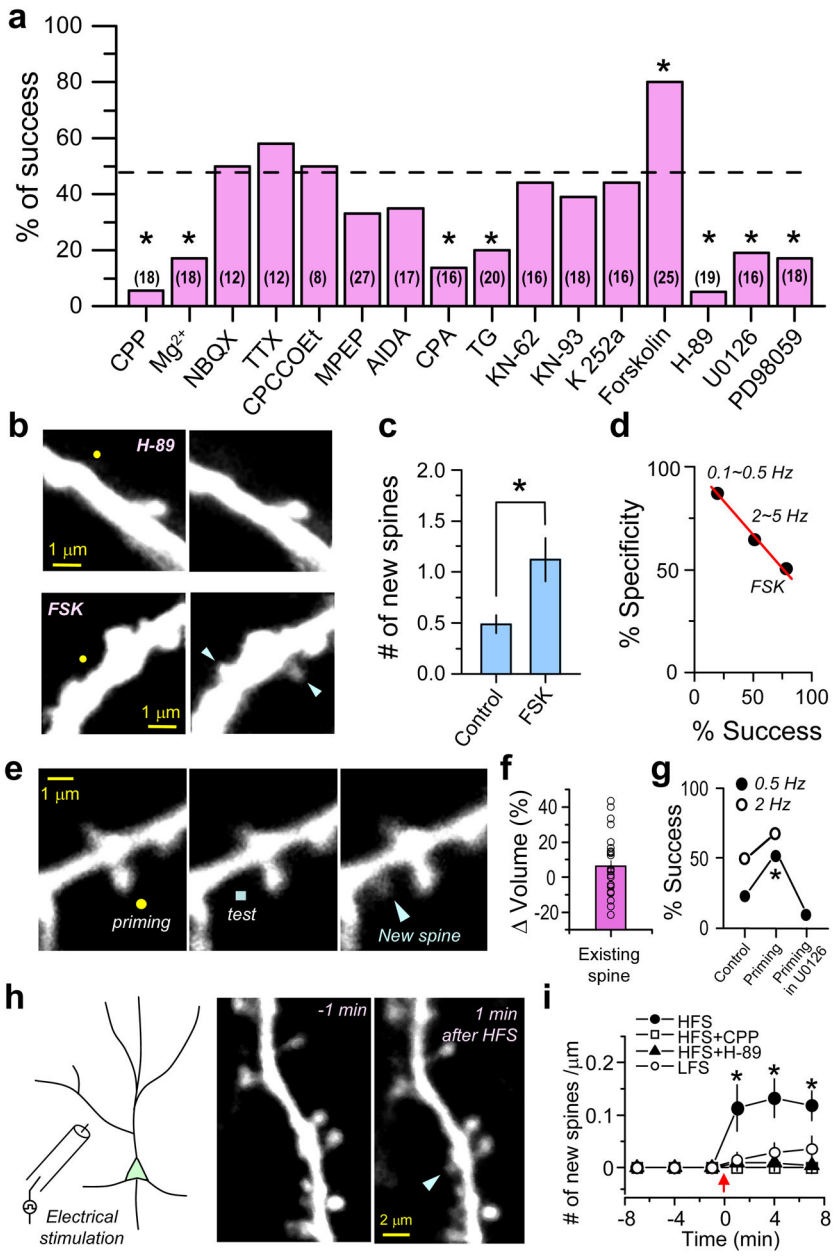


**Figure 3. Molecular mechanisms of glutamate-induced spine formation**

**(a)** Spine formation using the 40 pulses at 2 Hz protocol was tested in the presence of pharmacological agents. The dotted line indicates the success percentage in control conditions to which statistical comparison was made. The number of induction attempts for each condition is given in parentheses and the numbers of successes and total trials are summarized in the Supplemental Table 2. Acronyms were used for thapsigargin (TG) and cyclopiazonic acid (CPA).

**(b)** Examples of blockade of spine generation and of exuberant spine growth. Images taken before (*left*) and after (*right*) glutamate uncaging in the presence of either H-89 or forskolin (FSK). Arrowheads indicate nascent spines.

**(c)** Summary of the average number of new spines per induction attempt (Control: 0.48 ± 0.09, n=33; FSK: 1.12 ± 0.21, n=25, $p<0.005$).
**(d)** Inverse relationship between the location specificity and success rate. Data from three groups (0.1~0.5 Hz, 2~5 Hz, and FSK at 2 Hz) are plotted. Specificity was measured as the percentage of cases in which the spine arose within 1μm of the uncaging spot.
**(e)** Representative images of priming experiments in which 40 pulses of 2 Hz glutamate uncaging were delivered to a pre-existing spine (yellow circle) followed by an additional 40 pulses (0.5 Hz or 2 Hz) delivered to the nearby dendrite (blue square). Releasing glutamate did not cause enlargement of the pre-existing spine head (*left*), but did trigger new spine growth from the dendrite (*middle*, *right*).
**(f)** Changes in the fluorescence of preexisting spine heads exposed to the priming stimulus (individual spines:circles; bar graph:average±SEM) (n=31).
**(g)** Percentage of successful spine generation at the indicated test frequencies with and without priming. U0126 prevented spinogenesis facilitated by the priming protocol.
**(h)** Schematic of the experiment (*left*) and images of a dendrite 1 minute before (*middle*) and after (*right*) high-frequency electrical stimulation (HFS) (2×100 pulses at 100 Hz).
**(i)** Average numbers of new spines generated by HFS per micron of dendrite in control conditions (at 7 minutes: 0.12 ± 0.03, n=11, $p<0.005$), in the presence of CPP (0, n=8, $p>0.5$), or H-89 (0.004 ± 0.001, n=12; $p>0.5$). The same number of pulses at a lower frequency (LFS, 10 Hz) generated fewer new spines (0.035 ± 0.024, n=7, $p>0.1$). Error bars: SEM.

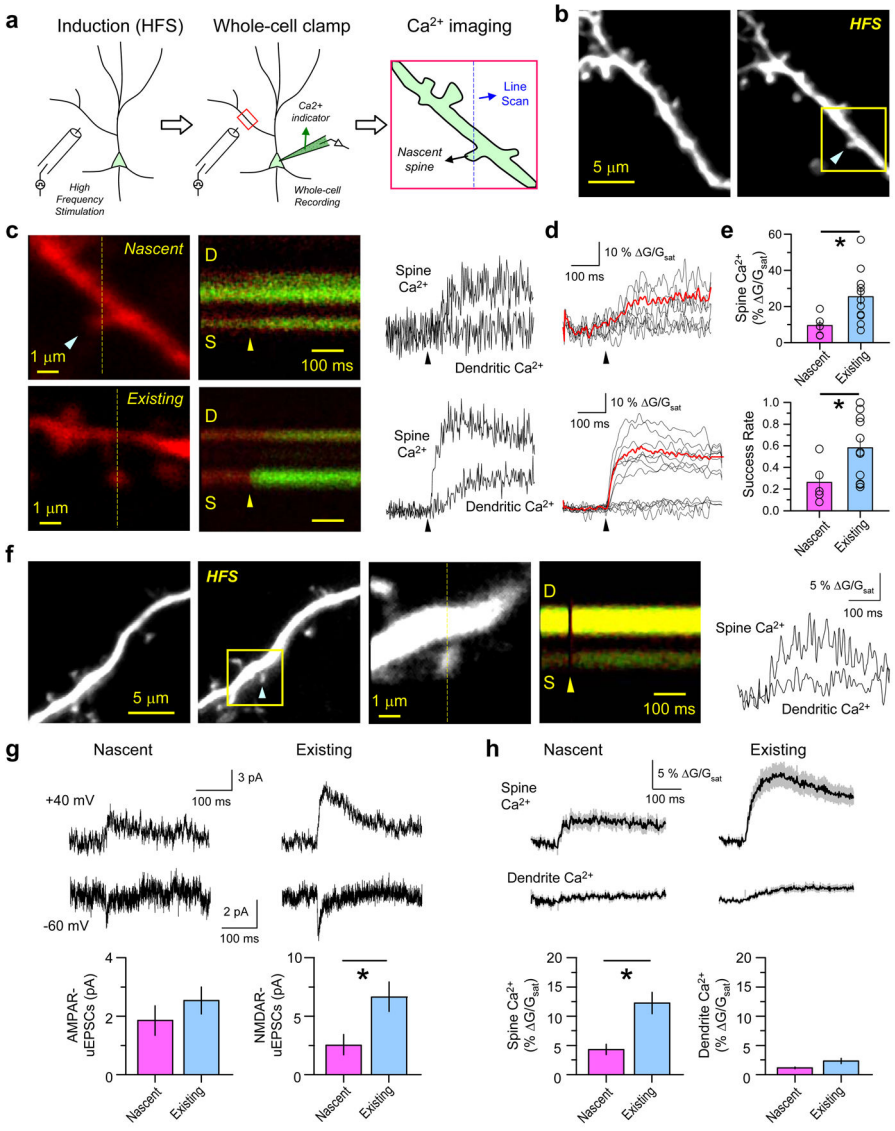


**Figure 4. Functional characterization of new spines**

**(a)** Schematic of the experimental procedure. HFS was delivered ~30 µm from the target dendritic region (red box). After nascent spines were identified, $Ca^{2+}$ indicator was loaded into the cell through a whole-cell recording pipette. The newly generated spine was examined at higher temporal and spatial resolution to measure synaptically-evoked $Ca^{2+}$ transients in the spine head and perform optical-quantal analysis.

**(b)** Images before and after HFS showing the new spine (arrowhead) and the area subsequently analyzed at higher resolution (yellow box).

**(c)** Images (*left*) of newly-generated (*top*) and pre-existing (*bottom*) spines filled with the fluorophore Alexa 594 (red, 20 µM) and Fluo-5F (green, 300 µM). Fluorescence was collected (*middle*) and quantified (*right*) from a line-scan intersecting the spine (S) and dendrite (D) following electrical stimulation (arrowhead). The increases in green fluorescence indicate $Ca^{2+}$ entry.

**(d)** Green fluorescence transients collected in consecutive trials (black) showing successes and failures. The average "success" fluorescence transient is also shown (red).
**(e)** Average amplitude (*top*, $\Delta G/G_{sat}$) and rate of success (*bottom*) of success trials in nascent and neighboring existing spines for neurons held at −60 mV (nascent and existing: Spine $Ca^{2+}$ $G/G_{sat}$: 9.45 ± 2.8 %, n = 5, 25.5 ± 4.4 %, n = 11, $p<0.05$; Success rate: 0.26 ± 0.09, n = 5, 0.58 ± 0.09 %, n = 11, $p<0.05$).
**(f)** Similar experiments as those in **a-c** using glutamate uncaging to characterize the glutamate receptors on the nascent spine.
**(g)** Examples (*top*) and average amplitudes (*bottom*) of AMPAR- and NMDAR-mediated uEPSCs at holding potentials of −60 and +40 mV, respectively, using 1 ms uncaging pulses. (nascent and existing: AMPAR-uEPSC: −1.9 ± 1.4 pA, n = 8, −2.5 ± 0.5 pA, n = 18, $p>0.05$; NMDAR-uEPSC: 2.5 ± 1.4 pA, n = 8, 6.3 ± 1.3 pA, n = 18, $p<0.05$).
**(h)** Average $Ca^{2+}$ transients measured in spine heads and dendrites for neurons held at −60 mV (nascent and existing: Spine $Ca^{2+}$ $\Delta G/G_{sat}$: 4.3 ± 0.9 %, n = 8, 12.3 ± 1.8 %, n = 18, $p<0.05$; Dendrite $Ca^{2+}$ $\Delta G/G_{sat}$: 1.1 ± 0.1 %, n = 8, 2.3 ± 0.4 %, n = 18, $p>0.05$). Error bars: SEM.